American Journal of Polymer Science 2014, 4(3): 63-72
DOI: 10.5923/j.ajps.20140403.01

Novel Water Purification Membranes of Polystyrene/ Multi-Walled Carbon Nanotube-*grafted*-Graphene Oxide Hybrids

Ayesha Kausar

Nanosciences and Catalysis Division, National Centre For Physics, Quaid-i-Azam University Campus, Islamabad, Pakistan

Abstract In this work, thin nanocomposite membranes were designed for water desalination. For the purpose, pristine polystyrene (PS) was modified into amino-functional polystyrene (PS-NH_2) and used as matrices. Nano-bifiller technology has been employed involving the formation of multi-walled carbon nanotube-*grafted*-graphite oxide (MWCNT-*g*-GO). Prior to grafting, nanotubes were acid functionalized to chemically interact with GO. Consequently, nanocomposite series with 0.1-3 wt. % nano-bifiller were prepared. Surface morphology of the membranes was studied by scanning electron microscopy. PS-NH_2/MWCNT-*g*-GO 0.1-3 hybrid showed increasing trend in tensile strength from 45.5-50.2 MPa relative to PS-NH_2/MWCNT-*g*-GO 0.1-3 (38.1-43.5 MPa). % Water content of PS-NH_2/MWCNT-*g*-GO series was changed from 1.58 to 1.94 % whereas for PS/MWCNT-*g*-GO hybrids altered in the range of 2.22-3.78 %. Moreover, PS-NH_2/MWCNT-*g*-GO 3 showed highest porosity in water as 0.20 gcm^{-1} among all membranes. Shrinkage ratio decreased with increasing nano-bifiller content in all prepared hybrid membranes. Pure water flux and membrane recovery (12.3 $mLcm^{-2}min^{-1}$ and 89.6 %) for of PS-NH_2/MWCNT-*g*-GO 3 were found to be higher than other membranes prepared.

Keywords Modified polystyrene, Multi-walled carbon nanotube-*grafted*-graphite oxide, Hybrid membranes, Morphology

1. Introduction

At present, membrane filtration is recurrently employed technique for water purification [1]. Commendable membranes must present reduced thermal conductivity, amplified hydrophobicity and superior penetrability. Polymers or additives accompanied by the formation strategy of membrane have been accounted to engender such physiognomies. In order to purify through hydrophilic polymer membrane, surface charge and porosity exhibit crucial parts to eradicate various pollutants of kinds like microorganisms, organic contaminants and inorganic particles from the treatment of superfluous water [2, 3]. Innovative membrane processes have less energy costs, guileless operative control, prospective material recuperation and condescending compact congregation than traditional technology. In this regard, nanaofiltration membranes have procured interest on account of straightforward filtration methodologies and pore size [4]. However, the membrane technology bestows the drawback of mechanical hardness and fouling [5, 6]. Biological adsorbates like bacteria and virus have sizes of more than microporous adsorbents. Depending on the size dissimilarity, greatest amount of biological pollutants have un-approachability to the surface area of pores, restricting the removal [7, 8]. Recently, nanotechnology has industrialized various nanomaterials like multi-walled carbon nanofiller (MWCNT)/polymer-based nanocomposite, etc. that have the capacity to separate biological pollutants, heavy metals and organics [9, 10]. The modification of polymer membranes may amend the structure and composition of macromolecules [11]. Lately, polymer / MWCNT composites have revealed astonishing boost in their mechanical and thermal features specifically on well-dispersion of filler in the domains of matrix [12-14]. Generally, with the increase in crystalline comportment in polymers, the free volume available to species transport may decrease instigating an undesirable influence on the ultimate membrane transport features [15, 16]. High hydrophobicity creates additional contraction and influence the membrane porosity, reducing the clean water flow rate. The key factor is surface which interacts with the environment [17]. Convincingly, functionalization is desired for the application of polymer membranes [18]. Polystyrene (PS) is a multi-purpose and widely used polymer because of its good chemical resistance, the low density, and the ease of processing and can be used to decrease the exorbitant

* Corresponding author:
asheesgreat@yahoo.com (Ayesha Kausar)
Published online at http://journal.sapub.org/ajps

membrane shrinkage [19]. In our research we have chosen two types of nanofillers to reinforce modified polystyrene - based membranes. Firstly, MWCNT was opted which is an extensively used filler for the purpose. For application of MWCNT as additives in polymers, surface functionalization is important not only to simplify the fabrication process of polymer/MWCNT composites, but also to improve the interfacial bonding between the polymer matrix and the MWCNT. The nanotube has, thus, been functionalized with various functional groups to increase their water solubility and compatibility. Secondly, graphene oxide (GO) owing to its better reinforcement properties in polymer matrix even at lower loading level [20]. Our motivation to utilize graphene oxide in preparing the filtration membrane actually stems from the unique properties that GO possesses owing to its functional groups such as carboxyl, epoxy, and hydroxyl groups. The presence of GO in membrane material would induce hydrophilicity, which may ensure high water permeation and impede bio-fouling because of the low interfacial energy between a surface and water. To enhance the interfacial compatibility between PS and nanofillers, we have also modified polystyrene with amino-functionality (PS-NH_2). The graphene oxide was then grafted with nanotubes (MWCNT-*g*-GO). Using the bi-filler in varying content (0.1-3 wt. %), series of PS/MWCNT-*g*-GO and PS-NH_2/MWCNT-*g*-GO were fabricated. Tensile properties, morphology, % solvent content, porosity, shrinkage ratio, pure water flux, salt rejection, and membrane recovery were scrutinized.

2. Experimental Section

2.1. Materials

Polystyrene (average M_w~350,000, average M_n~170,000), polyethylene glycol (average M_w ~ 8,000), graphite (fine powder), anhydrous tin(II) chloride (99 %), potassium persulfate ($K_2S_2O_8$, 99 %), and phosphorus pentoxide (P_2O_5, 99 %) were obtained from Aldrich. Multi-walled carbon nanotube > 98% carbon basis, O.D. × L 6-13 nm × 2.5-20 μm (chemical vapor deposition method) was also prepared from Aldrich. Sodium hydroxide (NaOH, 98%), tetrahydrofuran (THF, 99%), methanol (99%), ethanol (99 %), hydrochloric acid (HCl, 99 %), nitric acid (HNO_3, 65 %) and sulfuric acid (H_2SO_4, 98%) were supplied by Merck.

2.2. Instrumentation

The infrared (IR) spectra were recorded using a Fourier transform infrared (FTIR) Spectrometer, Model No. FTSW 300 MX, manufactured by BIO-RAD, California, USA (4 cm^{-1} resolution). The field Emission Scanning Electron Microscopy (FE-SEM) of freeze fractured samples was performed using a JSM5910, JEOL Japan. The stress-strain behavior of the samples was studied using a Testomeric materials testing machine M500–30CT. The test specimens were employed in the form of strips (lwh 40×2×7 ± 0.05 mm^3) according to an ASTM D638 standard method. The crosshead speed was 2 mm/min at room temperature. The data given are the average of the three measurements. To analyze the water content, membranes were soaked in distilled water for 24 h followed by mopping with blotting paper and weighing. The wet membranes were first kept at 100 °C for 24 h, and subsequently weighed to obtain the dry weight using an electronic balance. The percent solvent content was calculated using the following equation:

$$\% \text{ Solvent Content} = \frac{W_1 - W_2}{W_2}$$

Where W_1 = Wet membrane weight (g)
W_2 = Dry membrane weight (g)

To analyze the porosity of the membranes, samples were soaked in distilled water for 24 h followed by mopping with blotting paper and weighing. The membranes were dried at 100 °C for 24 h and weighed. Porosity was calculated using the equation:

$$\text{Porosity} = \frac{W_1 - W_2}{A_h}$$

Where W_1 = Wet membrane weight (g)
W_2 = Dry membrane weight (g)
A_h = Membrane area (cm^2)

Pure water flux of membrane was measured using membrane cell with cross-flow mode. The permeate was collected every 10 min for 1 h. Membrane after compaction, were subjected to pure water flux estimation at trans-membrane pressure of 345 kPa. The permeability was measured under steady state flow. Pure water flux was calculated as follows:

$$J_w = \frac{Q}{At}$$

Where Q = Quantity of permeate collected (L)
J_w = Pure water flux ($mLcm^{-2}$ min^{-1})
A = Membrane area (cm^{-2})
t = Sampling time (min)

A piece of wet membrane, immersed in a water bath, was cut and the length and width of the membrane was measured. Then the membrane was heated at 100 °C for 24 h. The length and width of the dry membrane were measured. The shrinkage ratio was calculated using the equation:

$$\text{Shrinkage ratio} = \left[1 - \left(\frac{ab}{a_o b_o}\right)\right].100$$

Where a = length of dry membrane (m)
b = breadth of dry membrane (m)
a_o = length of wet membrane (m)
b_o = breadth of wet membrane (m)

Rejection indicates the amount of components rejected by membranes. It shows the separation efficiency of the components by the membrane. It is calculated as:

$$R_e = 1 - \frac{Cp}{Cf}$$

Where Re = Rejection
Cp = Concentration of components in permeate (g/m^3)
Cf = Concentration of components in feed water (g/m^3)

Recovery is also known as productivity. Here also the membrane cell with cross-flow mode was used. According to mass balance, the feed flow is equal to the sum of concentrate flow and permeates flow. Recovery was calculated by:

$$\gamma = \frac{Qp}{Qf} . 100$$

Where, γ = Recovery (%)
Qp = Permeate flow (m^3/h)
Qf = Feed flow (m^3/h)

2.3. Preparation of Graphene Oxide (GO)

The graphite powder (15 g) was put into a solution of concentrated H_2SO_4 (60 mL), $K_2S_2O_8$ (7.8 g), and P_2O_5 (8.4 g) and refluxed at 80 °C. After 2 h, the mixture was left to cool down to room temperature for 6 h. The mixture was then carefully diluted with 300 mL of distilled water, filtered, and washed until the pH became neutral. The product was dried at 60 °C for 48 h [21].

2.4. Purification of Raw MWCNT

Purification steps involved oxizing 20 g raw MWCNT at 420 °C for 0.5 h. 18 g oxidized MWCNT were then sonicated by adding 300 mL HCl in a 500 mL two necked round bottom flask. The flask was sonicated for 3h at room temperature. 0.45 nm size Whatman filter paper was used to filter the nanotubes through suction a filtration assembly, followed by washing with distilled water to attain pH ~7. As filtered MWCNT were dried at 90 °C for 4 h.

2.5. Functionalization of MWCNT

17 g MWCNT was added to 10 mL H_2SO_4:HNO_3 mixture (3:1), and then sonicated and refluxed for 4 h at 50 °C. The above mixture was then filtered and washed with distilled water till pH~7. Black product obtained was dried at 80 °C for 12 h. FTIR (KBr) 3426 cm^{-1} (O–H stretching vibration), 3021 cm^{-1} (aromatic C–H stretching vibration), 1720 cm^{-1} (C=O stretching vibration) [22].

2.6. Multi-Walled Carbon Nanotube-*grafted*-Graphite Oxide (MWCNT-*g*-GO)

Initially, above prepared GO (0.5g) and acid functionalized MWCNT (0.5 g) were separately sonicated in 30 mL of deionized water for 8 h to attain uniform dispersion of the nanofillers. Then the two mixtures were added to 500 mL HNO_3. The acid mixture was again sonicated at 80 ºC for 8 h at room temperature and then centrifuged for 4 h. The resulting MWCNT-*g*-GO hybrid was washed with deionized water and filtered [23]. Finally, the product was dried at 70 °C (Fig. 1).

2.7. Functionalization of Polystyrene (PS-NH_2)

The functionalization of polystyrene first involved the dissolution of 10 g of polystyrene in 50 mL of THF to form a stock solution. The nitrating mixture (70 mL fuming HNO_3 and 30 mL concentrated H_2SO_4) was added drop wise to the stock solution. The mixture was cooled to 0 °C and then refluxed at 60 °C for 6 h. The above mixture was cooled and neutralized with 30% solution of NaOH. The nitro-functionalized polymer obtained was dried at 80 °C for 24 h. 5 g of the nitro-functionalized polystyrene was then dissolved in 30 mL THF to form a stock solution. The reducing mixture was prepared by dissolving 60 g of the anhydrous stannous chloride in 60 mL of HCl. The polymer solution and the reducing mixture were mixed and refluxed at 80 °C for 8 h. This mixture was also neutralized with the 30% NaOH. The orangish brown color polymer was obtained and dried at 80 °C [24].

2.8. Preparation of PS/MWCNT-*g*-GO and PS-NH_2/MWCNT-*g*-GO Membranes

The series of the hybrid membranes were prepared with the nano-bifiller. 1g of polystyrene (PS/PS-NH_2), was dissolved in 10 mL of THF to prepare the stock solution with a stirring of 12 h. The MWCNT-*g*-GO (0.1, 0.3, 1 and 3 %) was added to the stock solution and stirred for another 12 h. Thin hybrid films were cast in the glass Petri dishes [25].

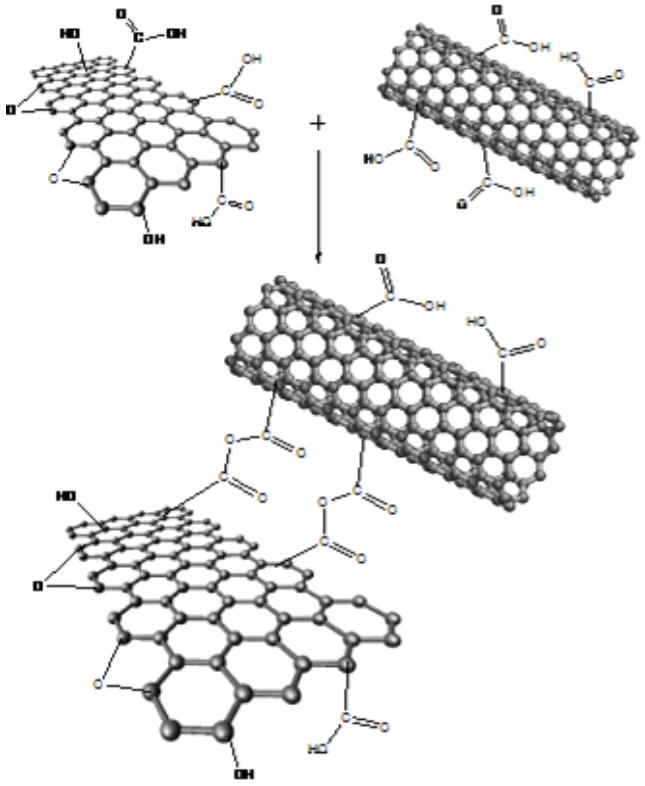

Figure 1. Schematic illustration for the formation of multi-walled carbon nanotube-*grafted*-graphene oxide

3. Results and Discussion

3.1. FTIR Analysis

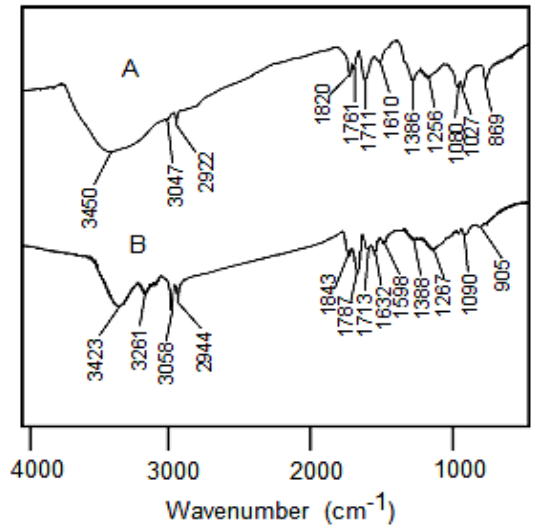

Figure 2. FTIR spectra of (A) PS/MWCNT-*g*-GO 0.1 and (B) PS-NH_2/MWCNT-*g*-GO 0.1 hybrids

Fig. 2A shows the FTIR spectrum of PS/MWCNT-*g*-GO 0.1 hybrid membrane. All the expected vibrations were found to appear in the spectrum and corroborated the structure of novel membranes. The ester bands were found to appear at 1711 and 1256 cm^{-1} due to chemically linked nano-bifiller. Furthermore, the C=O anhydride stretching vibrations were also observed at 1820 and 1761 cm^{-1} because of the reinforcement introduced. Aromatic and aliphatic C–H also appeared at 3047 and 2922 cm^{-1} respectively, owing to the polystyrene spine. Peaks due to un-oxidized graphite structure and aromatic C=C were found to appear at 1610 cm^{-1}. FTIR spectrum of PS-NH_2/MWCNT-*g*-GO 0.1 hybrid membrane is shown in Fig. 2B. In the case of amino-functional polystyrene matrix, aromatic N-H stretching and bending vibrations were found to appear at 3261 and 1598 cm^{-1} respectively. The ester peaks appear at 1713 and 1267 cm^{-1}, similar to PS/MWCNT-*g*-GO 0.1 hybrid. Moreover, the anhydride C=O stretching vibrations were also observed at 1843 and 1787 cm^{-1}. The broad –OH stretching vibrations at 3450 and 3423 cm^{-1} were seen in both the PS/MWCNT-*g*-GO and PS-NH_2/MWCNT-*g*-GO spectra respectively.

3.2. Mechanical Properties

Table 1 shows the tensile properties of the neat polystyrene, the modified polystyrene, PS/MWCNT-*g*-GO and PS-NH_2/MWCNT-*g*-GO hybrids. The pure polystyrene and the amino-functional polystyrene illustrated comparatively lower tensile strength of 20.3 and 25.7 MPa relative to the hybrid series. The tensile modulus and toughness of the PS and PS-NH_2 was found to be lower around 0.7 and 0.9 GPa and 0.14 and 0.15 Jm^{-3} respectively. Even as examining the effect of the nano-bifiller loading on the tensile strength, the PS/MWCNT-*g*-GO 0.1-3 was found to have lower values in the tensile strength (38.1-43.5 MPa) relative to the PS-NH_2/MWCNT-*g*-GO 0.1-3 (45.5-50.2 MPa). Dependence of the tensile strength of PS-NH_2/MWCNT-*g*-GO 0.1-3 on the nano-bifiller content is given in the Fig. 3. The most probable reason was the increased robustness of the amino-functional matrix after the modification and the hybrid formation. However, the filler loading in the matrices (PS and PS-NH_2) resulted in the higher mechanical stability compared with the pure polymers. The tensile modulus and toughness of PS-NH_2/MWCNT-*g* -GO was also found to be higher in the range 7.4-10.7 GPa and 999-1234 Jm^{-3} respectively. The tensile modulus and toughness of PS/MWCNT-*g*-GO was relatively lower in the range 3.1-5.2 GPa and 720-1033 Jm^{-3} respectively.

On the other hand, the pristine and the modified polymers without the nano-filler have relatively less rigid structure. Although the elongation at break showed decreasing trend with increased filler loading in both the hybrid series. In PS/MWCNT-*g*-GO series, the elongation at break decreased from 8.8 to 5.2 %, while PS-NH_2/MWCNT-*g*-GO 0.1-3 showed decrease from 7.5 to 4.4 % due to increased matrix/filler amalgamation. When the tensile strength of the novel PS-NH_2/MWCNT-*g*-GO membranes was compared with a sample of HDPE/PVC (90:10), the tensile strength of 49 MPa, modulus of 1.13 G and toughness value of 96 Jm^{-3} was obtained. The properties of PS-NH_2/MWCNT-*g*-GO were found to be considerably higher than the HDPE/PVC composition prepared.

Table 1. Mechanical properties of PS, PS-NH_2, PS/MWCNT-*g*-GO and PS-NH_2/MWCNT-*g*-GO hybrids

Composition	Tensile Strength (MPa)	Elongation at break	Tensile Modulus (GPa)	Toughness (Jm^{-3})
PS	20.3	0.02	0.7	0.14
PS-NH_2	25.7	0.02	0.9	0.15
PS/MWCNT-*g*-GO 0.1	38.1	8.8	3.1	720
PS/MWCNT-*g*-GO 0.3	39.2	7.5	3.8	832
PS/MWCNT-*g*-GO 1	41.2	6.9	4.1	921
PS/MWCNT-*g*-GO 3	43.5	5.2	5.2	1033
PS-NH_2/MWCNT-*g*-GO 0.1	45.5	7.5	7.4	999
PS-NH_2/MWCNT-*g*-GO 0.3	47.8	6.2	8.2	1032
PS-NH_2/MWCNT-*g*-GO 1	48.9	5.3	9.1	1145
PS-NH_2/MWCNT-*g*-GO 3	50.2	4.4	10.7	1234

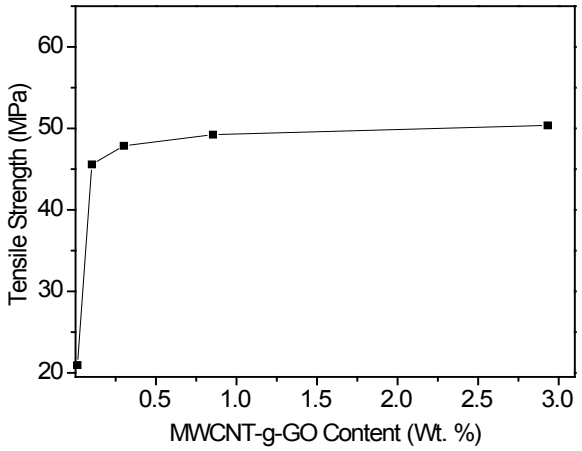

Figure 3. Drift of tensile strength *vs.* MWCNT-*g*-GO content in PS-NH_2/MWCNT-*g*-GO hybrids

3.3. Morphology Investigation

FE-SEM analysis was performed for PS/MWCNT-*g*-GO 0.1, PS-NH_2/MWCNT-*g*-GO 0.1 and PS-NH_2/MWCNT-*g*-GO 3. The Fig. 4A-C shows the morphology of pure polystyrene matrix loaded with the 0.1 wt. % MWCNT-*g*-GO. The surface morphology reflected the layered structural arrangement. Fig. 5A-E shows the morphology of amino-functional polystyrene loaded with 0.1 and 1 wt. % MWCNT-*g*-GO. The micrographs of PS-NH_2/ MWCNT-*g*-GO 0.1 at various resolutions (Fig. 5A & B) have shown the complete embedding of nano-bifiller in the matrix probably due to the lower filler loading. The fractured membrane surface of PS-NH_2/MWCNT-*g*-GO 1 (Fig. 5C-D) also showed the polymer coating over the entire nano-bifiller loaded. The nano-bifiller coated with polymer was more visible in the micrographs of PS-NH_2/MWCNT-*g*-GO 3 at 500 nm-1µm (Fig. 6 A & B). Such type of folded and layered morphology is usually observed for polymer/graphene nanocomposites [26]. However, the closer cross section image of PS-NH_2/MWCNT-*g*-GO 3 at 200 nm showed the nanoporous morphology of the membranes (Fig. 6C). The nanoporous morphology was consistent with the membrane property studies reported in the succeeding sections.

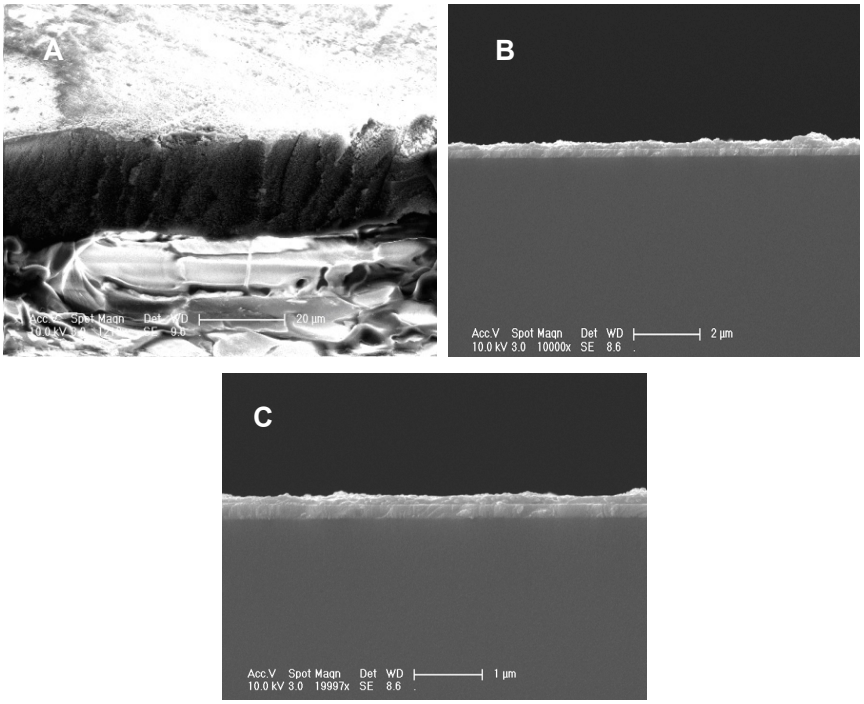

Figure 4. FESEM micrographs of (A) PS/MWCNT-*g*-GO 0.1 at 20 µm; (B) PS/MWCNT-*g*-GO 0.1 at 2 µm; (C) PS/MWCNT-*g*-GO 0.1 at 1 µm

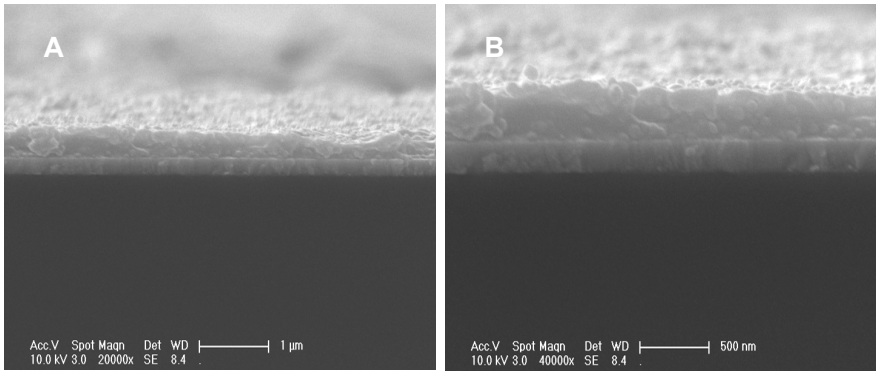

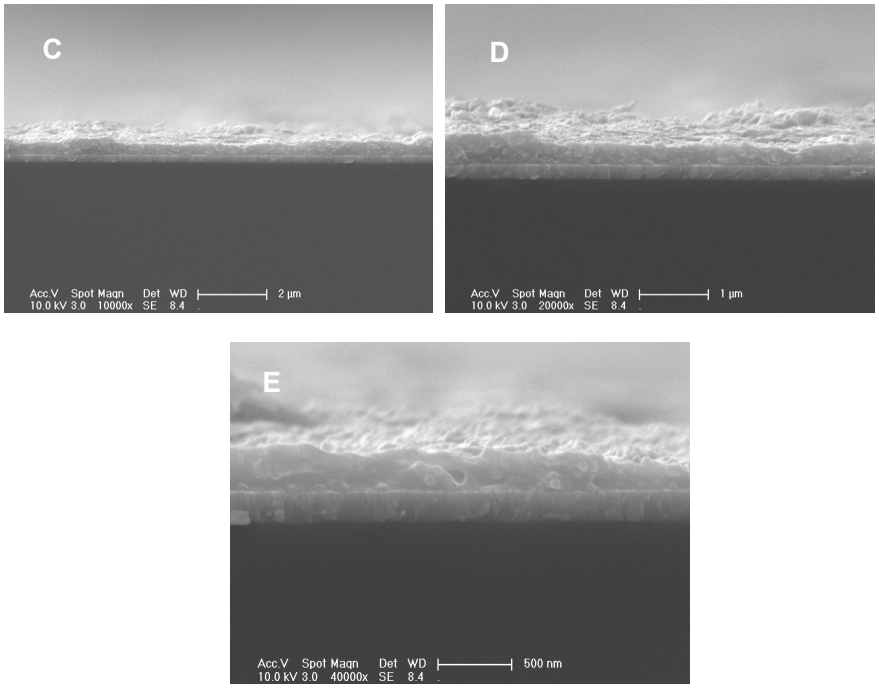

Figure 5. FESEM micrographs of (A) PS-NH_2/MWCNT-*g*-GO 0.1 at 1 µm; (B) PS-NH_2/MWCNT-*g*-GO 0.1 at 500 nm; (C) PS-NH_2/MWCNT-*g*-GO 1 at 2 µm; (D) PS-NH_2/MWCNT-*g*-GO 1 at 1 µm; and (E) PS-NH_2/MWCNT-*g*-GO 1 at 500 nm

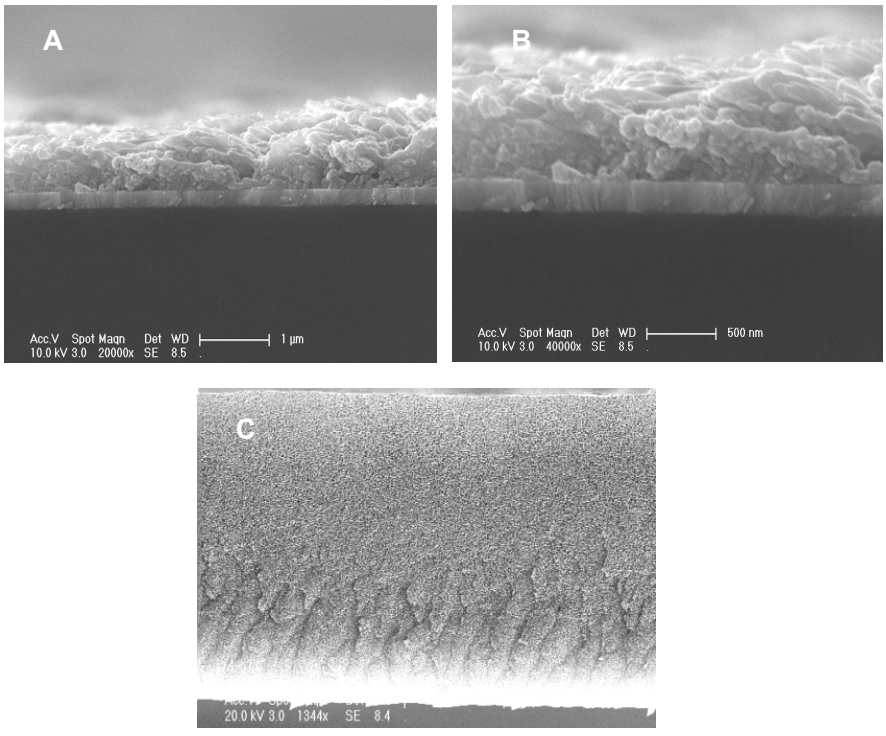

Figure 6. FESEM micrographs of (A) PS-NH_2/MWCNT-*g*-GO 3 at 1 µm; (B) PS-NH_2/MWCNT-*g*-GO 3 at 500 nm; and (C) PS-NH_2/MWCNT-*g*-GO 3 at 200 nm (cross section)

3.4. Membrane Properties

Porosity of PS, PS-NH_2, PS/MWCNT-*g*-GO and PS-NH_2/MWCNT-*g*-GO membranes are reported in Table 2. Neat PS membrane had lower porosity in all the solvents tested ~ 0.001 g/cm^2. The membranes showed a steady increase in porosity with nano-bifiller content in different solvents (water, ethanol, methanol and propanol). This is because the nano-filler enhanced the hydrophilic nature of the membranes. As the hydrophilicity of solvent decreased (moving from water to propanol) the membrane porous nature was also decreased. % Solvent content of membranes

was also measured and found to show increasing trend in different solvents (Table 3). However, % solvent content was also observed to decline when moving from water to less polar solvent depending upon the solvent hydrophilicity. Both the porosity (0.20 g/cm^2) and percent solvent content (3.78 %) was dependent upon the solvent hydrophilicity and the best results were found when membranes were tested in water. Moreover, the decrease in shrinkage ratio has high impact on the membrane porosity. Higher porosity resulted in lower shrinkage ratio of the membranes. Table 4 shows that as the nano-bifiller content increased from 0.1-3 wt. % the shrinkage ratio decreased accordingly with the increased filler. This was attributed to the fact that the loading enhanced the porous nature of membranes. PS/MWCNT-*g*-GO 0.1-3 showed decrease in shrinkage ratio from 8.61-7.43, while PS-NH_2/MWCNT-*g*-GO showed decrease in shrinkage ratio from 8.33-7.31 in water. Pure PS and modified matrices have shrinkage ratio of 10.9 and 9.80 respectively.

Pure water flux was also measured as an important nano-filtration membrane feature. Here, the water flux was increased with the augmented nano-bifiller content due to increased membrane porosity. The modified PS membrane PS-NH_2/MWCNT-*g*-GO 3 showed higher water flux of 12.3 mLcm^{-2} min^{-1} relative to PS/MWCNT-*g*-GO 3 with 9.2 mLcm^{-2} min^{-1}. Moreover, salt (NaCl) rejection has higher values for PS-NH_2/MWCNT-*g*-GO 3 membrane as compared to PS/MWCNT-*g*-GO 3 showing better membrane performance. Membrane recovery was also maximum for PS-NH_2/MWCNT-*g*-GO 3~89.6%. The over all performance of 3 wt. % filler loaded PS-NH_2/MWCNT-*g*-GO membrane was better than other composites prepared. The salt rejection efficiency of HDPE/PVC (90:10) was found to be 60 % which was lower than the novel membranes prepared. However, the flux was found to be 12 mLcm^{-2} min^{-1} which was slightly lower than that of PS-NH_2/MWCNT-*g*-GO 3 [27]. Another important aspect of the novel membranes was their high efficiency of absorption and retention of oil (fuel and compressor) and grease. The PS-NH_2/MWCNT-*g*-GO 3 membrane was tested for the de-oiling or removal of free and dispersed oil present in water. Higher oil removal efficiency of PS-NH_2/MWCNT-*g*-GO 3 at water flux of 12.3 mLcm^{-2} min^{-1} was observed. The membrane was found to be 94 % efficient in absorption of oil from water and 99 % for the grease removal. The performance of these membranes was not decreased at high temperatures (Table 6).

Table 2. Porosity of PS, PS-NH_2, PS/MWCNT-*g*-GO and PS-NH_2/MWCNT-*g*-GO membranes in different solvents

Concentration	Water	Ethanol	Methanol	Propanol
PS	1.01	0.006	0.003	0.001
PS-NH_2	1.16	0.87	0.76	0.25
PS/MWCNT-*g*-GO 0.1	1.58	0.78	0.66	0.34
PS/MWCNT-*g*-GO 0.3	1.66	0.81	0.71	0.45
PS/MWCNT-*g*-GO 1	1.89	1.13	0.92	0.57
PS/MWCNT-*g*-GO 3	1.94	1.38	1.01	0.64
PS-NH_2/MWCNT-*g*-GO 0.1	2.22	1.82	0.95	0.75
PS-NH_2/MWCNT-*g*-GO 0.3	2.73	1.99	1.15	0.77
PS-NH_2/MWCNT-*g*-GO 1	3.21	2.79	1.73	1.18
PS-NH_2/MWCNT-*g*-GO 3	3.78	2.82	1.93	1.43

Table 3. % Solvent content of PS, PS-NH_2, PS/MWCNT-*g*-GO and PS-NH_2/MWCNT-*g*-GO membranes in different solvents

Concentration	Porosity (g/cm^2)			
	Water	Ethanol	Methanol	Propanol
PS	0.001	0.001	0.001	0.001
PS-NH_2	0.02	0.02	0.005	0.004
PS/MWCNT-*g*-GO 0.1	0.04	0.03	0.008	0.007
PS/MWCNT-*g*-GO 0.3	0.05	0.04	0.01	0.009
PS/MWCNT-*g*-GO 1	0.07	0.05	0.03	0.01
PS/MWCNT-*g*-GO 3	0.08	0.06	0.05	0.02
PS-NH_2/MWCNT-*g*-GO 0.1	0.09	0.07	0.06	0.04
PS-NH_2/MWCNT-*g*-GO 0.3	0.10	0.08	0.07	0.06
PS-NH_2/MWCNT-*g*-GO 1	0.14	0.09	0.09	0.08
PS-NH_2/MWCNT-*g*-GO 3	0.20	1.13	0.10	0.09

Table 4. Shrinkage ratio of PS, PS-NH_2, PS/MWCNT-*g*-GO and PS-NH_2/MWCNT-*g*-GO membranes in different solvents

Concentration	Water	Ethanol	Methanol	Propanol
PS	10.9	9.11	8.72	8.12
PS-NH_2	9.80	8.92	7.74	6.90
PS/MWCNT-*g*-GO 0.1	8.61	7.61	7.12	6.62
PS/MWCNT-*g*-GO 0.3	8.22	7.52	6.82	6.43
PS/MWCNT-*g*-GO 1	7.60	6.94	5.24	5.11
PS/MWCNT-*g*-GO 3	7.43	5.27	48.4	4.90
PS-NH_2/MWCNT-*g*-GO 0.1	8.33	7.31	7.03	6.11
PS-NH_2/MWCNT-*g*-GO 0.3	8.12	7.11	6.67	5.14
PS-NH_2/MWCNT-*g*-GO 1	7.43	6.54	5.06	4.98
PS-NH_2/MWCNT-*g*-GO 3	7.31	5.03	4.24	4.65

Table 5. Pure water flux, salt rejection, and recovery of PS, PS-NH_2, PS/MWCNT-*g*-GO and PS-NH_2/MWCNT-*g*-GO membranes

Membrane type	Pure water flux ($mLcm^{-2}\ min^{-1}$)	Salt rejection (%)	Recovery (%)
PS/MWCNT-*g*-GO 1	8.4	56.5	72.7
PS/MWCNT-*g*-GO 3	9.2	62.2	80.2
PS-NH_2/MWCNT-*g*-GO 1	10.5	75.1	85.4
PS-NH_2/MWCNT-*g*-GO 3	12.3	80.3	89.6

Table 6. Performance of PS-NH_2/MWCNT-*g*-GO 3 membrane in treatment of oil and oil products

Sample	Before treatment (ppm)	After treatment (ppm)	Overall removal (%)
Fuel oil	72	4.0	94
Compressor oil	72	4.0	94
Grease	80	1.5	99

4. Conclusions

The effort involves the synthesis of modified polymers with well-defined structure as tailored membrane materials. The advanced surface functionalization yielded novel compatiblized barrier structures through the combination of modified polymer structure with tailored nano-filler. Once a satisfactorily selective polymer was found, a membrane was developed with a separating layer thin enough to obtain a high permeate flux. Important innovation was based on intrinsic properties of the polystyrene as a homogenous barrier phase and the formation of special morphologies by phase separation and pore formation in the barrier phase. The explicit properties of the boundary layers of the interphase region were, therefore, obtained. The formation of the specific interphase region through the integration of the modified surface and inclusion of tailored nano-additives into the continuous technical manufacturing of membranes has the advantage, that no additional process step would be necessary. A high surface activity, thus, resulted in low additional material cost. Due to the interplay between barrier and interphase properties of a membrane, such a *membrane modification* in reality is equivalent to the development of a novel membrane for large industrial units. This work, so, develops the design and operation of novel nanocomposite polystyrene/MWCNT-*g*-GO membranes for nano-filtration unit. Integrally skinned membranes can be obtained by casting novel polymer solution followed by an evaporation step. Due to evaporation of the solvent the surface concentration becomes high enough resulting in a thin dense layer, while underneath the top layer, where the polymer concentration is much lower, a porous layer was formed. Optimum surface porosity results in a larger contribution of the material to the separation properties of the composite membrane. High water flux was obtained using higher filler content generating optimal membrane porosity. However, the flux of polystyrene/MWCNT-*g*-GO membranes decreased with decreasing porosity, but is still acceptable. Further modified membranes can be developed with higher porosity and water flux. The properties of novel water purification membranes of PS-NH_2/MWCNT-*g*-GO after several uses seemed not to have changed when comparing the new membrane. The swelling of the membrane was found to be lower for the re-used membrane. Simultaneously, the water flux, salt rejection, and recovery of the re-used membranes was measured and found to be equally good. This indicates that the reliability of nano-bifiller technology in the maintenance of membrane structure and durability by applying several operational cycles of compressed water. Homogeneous dense membranes possess sufficient mechanical strength with a negligible contribution to the overall transport resistance. Another potential advantage of

the membranes was their resistance and resilience to the severe environmental conditions. The membrane damage might be caused by the heat generation occurring within the membrane or by degradation due to the alkaline environment or pressure created by the water filtration process. Howbeit, successive measurements with the same membrane sample demonstrate that this do not result in any damage of the membrane. Treatment of water using PS-NH_2/ MWCNT-g-GO 3 membrane for the oil recovery from water with high oil content was also an important aspect to meet beneficial use specifications. Due to high salt rejection efficiency, these membranes can also be used for example in electrodialysis where a salt solution is separated into a solution enriched in ions and a solution depleted of ions. According to the study of nanotoxicity, exposure to tailored nanoarchitectures might pose tangible human health risks. Although in the case of the novel membranes, the nano-filler was loaded at very low concentrations 0.1-3 wt. % embedded in the nontoxic polymer. Use of PS-NH_2 with such low nano-filler content is not supposed to cause any health risk.

REFERENCES

[1] Cornelissen, E.R., Boomgaard Th, van den., Strathmann, H., 1998, Physicochemical aspects of polymer selection for ultrafiltration and microfiltration membranes. Colloids Surf. A., 138(2-3), 283-289.

[2] McCutcheon, J.R., Elimelech, M., 2008, Influence of membrane support layer hydrophobicity on water flux in osmotically driven membrane processes. J. Membr. Sci., 318(1-2), 458-466.

[3] Evuti, A.M., Lawal, M., 2011, Recovery of coagulants from water works sludge: A review. Adv. Appl. Sci. Res., 2(6), 410-417.

[4] Bruggen, B.V.D., Vandecasteele, C., Gestel, T.V., Doyen, W., Leysen, R., 2003, A review of pressure-driven membrane processes in wastewater treatment and drinking water production. Environ. Prog., 22(1), 46-56.

[5] Ng, K.C., Saha, B.B., Chakraborty, A., Koyama, S., 2008, Adsorption desalination quenches global thirst. Heat Trans. Eng., 29(10), 845-848.

[6] Pianta, R., Boller, M., Urfer, D., Chappaz, A., Gmünder, A., 2000, Costs of conventional vs. membrane treatment for karstic spring water. Desalination, 131(1-3), 245-255.

[7] Suzuki, M., 1991, Application of fiber adsorbents in water treatment. Water Science and Technology, 23(7-9), 1649-1658.

[8] Harwood, V.J., Levine, A.D., Scott, T.M., Chivukula, V., Lukasik, J., Farrah, S.R., Rose, J.B., 2005, Validity of the indicator organism paradigm for pathogen reduction in reclaimed water and public health protection. Appl. Env. Microb., 71(6), 3163-3170.

[9] Li, Q., Mahendra, S., Lyon, D.Y., Brunet, L., Liga, M.V., Li, D., Alvarez, P.J., 2008, Antimicrobial nanomaterials for water disinfection and microbial control: potential applications and implications. Water res., 42(18), 4591-4602.

[10] Tena, A., Fernández, L., Sánchez, M., Palacio, L., Lozano, A.E., Hernández, A., Prádanos, P., 2010, Mixed matrix membranes of 6FDA-6FpDA with surface functionalized γ-alumina particles. An analysis of the improvement of permselectivity for several gas pairs. Chem. Eng. Sci., 65(6), 2227-2235.

[11] Feil, H., Bae, Y.H., Feijen, J., Kim, S.W., 1991, Molecular separation by thermosensitive hydrogel membranes. J. memb. Sci. 64(3), 283-294.

[12] Levi, N., Czerw, R., Xing, S., Iyer, P., Carroll, D.L., 2004, Properties of polyvinylidene difluoride-carbon nanotube blends. Nano Lett., 4(7), 1267-1271.

[13] Rao, G.P., Lu, C., Su, F., 2007, Sorption of divalent metal ions from aqueous solution by carbon nanotubes: A review. Separat. Purif. Tech., 58(1), 224-231.

[14] Di, Z.C., Ding, J., Peng, X.J., Li, Y.H., Luan, Z.K., Liang, J., 2006, Chromium adsorption by aligned carbon nanotubes supported ceria nanoparticles. Chemosphere, 62(62), 861-865.

[15] Brad-Estévez, A.S., Kang, S., Elimelech, M., 2008, A single walled carbon nanotube filter for removal of viral and bacterial pathogens. Small, 4(4), 481-484.

[16] Koo, K.K., Inoue, T., Miyasaka, K., 1985, Toughened plastics consisting of brittle particles and ductile matrix. Polym. Eng. Sci., 25(12), 741-746.

[17] de las Heras Alarcón C., Pennadam, S., Alexander, C., 2005, Stimuli responsive polymers for biomedical applications. Chem. Soc. Rev., 34(3), 276-285.

[18] Wienk, I.M., Boom, R.M., Beerlage, M.A.M., Bulte, A.M.W., Smolders, C.A., Strathmann, H., 1996. Recent advances in the formation of phase inversion membranes made from amorphous or semi-crystalline polymers. J. Membr. Sci., 113(2), 361-371.

[19] Xio, M., Sun, L., Liu, J., Li, Y., Gong K., 2002, Synthesis and properties of polystyrene/graphite nanocomposites. Polymer, 43(8), 2245-2248.

[20] Chao Xu, C., Cui, A., Xu, Y., Fu, X., 2013, Graphene oxide-TiO_2 composite filtration membranes and their potential application for water purification. Carbon, 62, 465–471.

[21] Kausar, A., Hussain, S.T., 2013, Effect of multi-walled carbon nanotubes reinforcement on the physical properties of poly (thiourea-azo-ether)-based nanocomposites. J. Plast. Film Sheet., 29(4), 365-383.

[22] Kausar, A., Hussain, S.T., 2013, Synthesis and properties of melt processed poly (thiourea-azo-sulfone)/carbon nanotubes nanocomposites. Chinese Journal of Polymer Science, 32(1), 64-72.

[23] Kausar, A., Hussain, S.T., 2014, Synthesis and properties of poly (thiourea-azo-naphthyl)/multiwalled carbon nanotube composites. J. Plast. Film Sheet., 30(1), 6-27.

[24] Kausar A., Zulfiqar, S., Ishaq, M., Sarwar, M.I., 2007, Mechanical properties of functionalized SEBS based inorganic hybrid materials. Polymer Bulletin, 59(4), 457–468

[25] Kausar, A., Hussain, A., Khan, M.Y., Siddiq, M., 2014, Fuel Cell Membranes Prepared from Multi-Walled Carbon Nanotubes and Silica Nanotubes Filled Sulfonated Polyamide/Sulfonated Polystyrene Porous Blend Films. J. Plast. Film Sheet., 30(3), 314-336.

[26] Guo-Hua, C., Da-Jun, W., Wen-Gui, W., Bin, H., Wen-li, Y., 2001, Preparation of polystyrene–graphite conducting nanocomposites via intercalation polymerization. Polym. Int., 50(9), 980-985.

[27] Tabatabaei, S. H., Carreau, P. J., Ajji, A., 2009, Microporous membranes obtained from PP/HDPE multilayer films by stretching. J. Membr. Sci., 345(1-2), 148–159.